Astron. Astrophys. 325, 1099–1114 (1997)

ASTRONOMY
AND
ASTROPHYSICS

Analytical studies of collimated winds

IV. Rotating and collimated MHD outflows

E. Trussoni[1], **K. Tsinganos**[2], **and C. Sauty**[3]

[1] Osservatorio Astronomico di Torino, Strada dell'Osservatorio 20, I-10025 Pino Torinese (TO), Italy
[2] Department of Physics, University of Crete and Research Center of Crete, P.O. Box 2208, GR-710 03 Heraklion, Crete, Greece
[3] Observatoire de Paris, DAEC, URA 173, F-92195 Meudon Cedex, France

Received 13 December 1996 / Accepted 24 Febraury 1997

Abstract. This paper continues the study of the initial acceleration and final collimation of magnetized and rotating astrophysical winds, via analytical and exact steady MHD solutions, self-similar in the meridional direction. By prescribing the shape of the streamlines on the poloidal plane for a nonspherically symmetric gas pressure, related *a posteriori* to the density via a nonconstant polytropic index γ relationship ($P \propto \rho^{\gamma}$), the main physical features of the outflowing plasma are deduced. Simple analytical relations show that cylindrical collimation and superAlfvénic terminal velocities can be attained asymptotically which depend on the rotation rate, the collimation distance from the base and the pressure gradient. If the plasma is overpressured at the flow axis, the pinching magnetic field can confine the jet, while if the gas is underpressured at its axis, the centrifugal force cannot always counterbalance the pinching magnetic stress and inwards pressure gradient. Physically acceptable solutions are obtained by a numerical integration of the radial dependence of the MHD system from the subAlfvénic to the asymptotically collimated regions and by a smooth crossing of the Alfvén critical surface. Two classes of solutions are found where either the flow speed increases monotonically to an asymptotic value, or it reaches a maximum value at an intermediate region. In the last case it is the toroidal magnetic field that collimates asymptotically the wind, while in the former the outflow of a slow rotator (respectively fast rotator) is collimated by the gas pressure (respectively by the magnetic field). The possible implications of these results on the modelling of astrophysical winds from slow and fast magnetic rotators are shortly discussed.

Key words: MHD – plasmas – Sun: atmosphere – solar wind – stars: atmosphere – ISM: jets and outflows

1. Introduction

It is commonly believed that collimated plasma outflows observed in many astrophysical environments, such as young stellar objects, symbiotic stars, compact galactic/extragalactic objects and AGN (e.g., see Ray 1996, Kafatos 1996, Biretta 1996, Mirabel & Rodriguez 1996), are driven by a combination of magnetocentrifugal forces and thermal pressure gradients in those rotating objects. Such combination of forces may effectively accelerate the outflows to large terminal speeds, while the toroidal magnetic field present in the asymptotic region and/or suitable gas pressure distributions there can effectively collimate them.

However, a self-consistent MHD modelling of these outflows is a rather complicated undertaking from the mathematical point of view and thence some approximations seem to be unavoidable. More specifically, in the framework of the assumptions of steadiness ($\partial/\partial t = 0$) and axisymmetry, the MHD equations reduce to the two well known Bernoulli and Grad-Shafranov (or transfield) equations, whose analytic treatment still remains at prohibitive levels. Heyvaerts & Norman (1989), through a detailed asymptotic analysis of this system, have shown that physically acceptable solutions ought to be collimated in the supersonic and superAlfvénic region, with similar results obtained by Appl & Camenzind (1992, 1993) in the relativistic regime. Complete solutions, connecting the base of the outflow to the asymptotic region and crossing smoothly the critical points have been obtained on the equatorial plane by arbitrarily neglecting the transfield equation (e.g., Weber & Davis 1967), close to the rotational axis by averaging the variables across the flow area (quasi 2-D approximation, see e.g. Lovelace et al. 1991) and fully numerically by Sakurai (1990).

An alternative quasi-analytical approach largely developed in the last years is to seek for solutions of the MHD system, with the so-called *self-similar* ansätz. The key to this technique is to express the physical variables as products of functions of the coordinates, with a prescribed scaling in one of them. In such a case the system of the MHD equations reduces to a set of ordinary differential equations. The choice of the scaling law depends on the astrophysical scenario under consideration (for details see Tsinganos et al. 1996). Such a treatment of outflows emerging from accretion disks has been explored follow-

Send offprint requests to: E. Trussoni (Torino)

ing the so-called *radial* self-similar symmetry, wherein the angle at which a given radial direction intersects all poloidal streamlines is fixed (Bardeen & Berger 1978, Blandford & Payne 1982, Contopoulos 1992, 1994, Li et al. 1992, 1995, Rosso & Pelletier 1994). The locations where the flow becomes superAlfvénic in these solutions lie on a *conical* surface and the gas velocity *decreases* with the angle from the rotational axis. This description, that also assumes a polytropic equation of state with a constant polytropic index, fails however on the rotational axis.

It occured to us to explore a new class of solutions by using the so called *meridional* self-similar ansätz, which is complementary to the above *radial* self-similarity. These solutions are suitable for describing the dynamics of an outflow emerging from a central body and its surrounding disk while at the same time they are valid close to its symmetry axis. The Alfvén surface is now *spherical* and the velocity *decreases* with the angle from the rotational axis. One notable aspect of this approach is that the constant γ polytropic equation of state is released. The structure of the streamlines is strictly related to the scaling law for the pressure. If the radial and meridional components of the gradient of the thermal pressure are independent, then the shape of the streamlines on the poloidal plane may be chosen *a priori* (e.g., conical, cylindrical, paraboloidal, etc., outflows). If, conversely, these two pressure components are assumed to be related, the poloidal structure of the streamlines is deduced from the solution of the full MHD system (for details see Sauty 1994, Trussoni et al. 1996).

In the framework of this treatment, we have investigated recently several classes of solutions, depending on whether or not the streamlines are prescribed *a priori*. In the former case, Low & Tsinganos (1986) and Tsinganos & Low (1989) analyzed the structure of *nonrotating* winds with nonradially expanding streamlines and assuming for the gas a spherically symmetric distribution of its density. This analysis was extended by including rotation and a non-spherically symmetric distribution of the density, for radially expanding hydrodynamic (Tsinganos & Trussoni 1990) or MHD winds (Tsinganos & Trussoni 1991, henceforth TT91). In a following treatment Trussoni & Tsinganos (1993, henceforth TT93) included collimation for nonrotating MHD outflows. In all these cases it has been shown that supersonic and superAlfvénic velocities can be obtained, albeit full collimation cannot be attained as it would require a divergent total heating rate in the plasma. Similar results were recently obtained by Rotstein & Ferro Fontán (1995a).

The alternative case in which the streamlines are self-consistently determined, by assuming a prescribed relation in the scaling of the various terms of the pressure, has been analyzed by Tsinganos & Sauty (1992a,b) for nonrotating flows, and by Sauty & Tsinganos (1994, henceforth ST94) by including rotation, albeit only for a spherically symmetric distribution of the pressure. The major novel result in this last case has been that superAlfvénic flows may be found with streamlines asymptotically either radial or fully collimated, and a criterion is presented for which of the two topologically distinct classes of outflows is obtained.

We complete here the analysis of TT91 and TT93 by seeking solutions for *rotating* outflows with a prescribed streamline pattern which asymptotivally becomes cylindrical. The outline of the paper is then as follows; in the next Sect. 2 we summarize the mathematical technique of the meridional self-similarity assumed in order to obtain the final equations. In Sect. 3 the asymptotic analytical results are discussed, while the numerical solutions are shown in detail in Sect. 4. The main features of the model and the astrophysical implications are discussed and summarized in Sect. 5.

2. A class of solutions for meridionally self-similar MHD outflows

Our starting point is the following well known set of ideal MHD equations describing the steady flow of an inviscid magnetized plasma with high electrical conductivity, in a spherically symmetric gravitational potential well created by a body a mass m,

$$\nabla \cdot \mathbf{B} = \nabla \cdot (\rho \mathbf{v}) = \nabla \times (\mathbf{v} \times \mathbf{B}) = 0$$

$$\rho(\mathbf{v} \cdot \nabla)\mathbf{v} - (\mathbf{B} \cdot \nabla)\mathbf{B}/4\pi = -\nabla(p + B^2/8\pi) - \mathscr{G}\frac{\rho m}{r^2}\mathbf{e}_r$$

$$\rho\mathbf{v} \cdot \left(\nabla h - \frac{\nabla P}{\rho}\right) = \rho\sigma\,, \qquad P = \frac{k_B}{\mu m_H}\rho T \tag{2.1}$$

where $\mathbf{B}$ and $\mathbf{v}$ are the magnetic field and the velocity, P, ρ and T are the gas pressure, density and temperature, h is the enthalpy, μ the mean molecular weight, m_H the proton mass, k_B Botzmann's constant, $\mathscr{G}$ the gravitational constant, and r the radial distance from the central body in the spherical coordinates (r, θ, ϕ).

In the last of Eqs. (2.1) $\rho\sigma$ denotes the volumetric rate of a net heating ($\sigma > 0$) or cooling ($\sigma < 0$) in the gas and it simply expresses energy conservation. For a complete solution of the problem one needs to further specify in this last equation the various heating/cooling sources and their quantitative expressions, see for example Hearn (1975), Vardavas & Hearn (1981). However, to this day we are not able to work out such a complete solution dealing adequately and simultaneously with the 2-D character and nonlinear dynamics of MHD flows, as well as with their detailed thermodynamics and energetics. This is because *first* the heating and cooling processes operating in the plasma and their exact expressions are poorly known in most cases of astrophysical interest such as those addressed in the context of this paper. And *second*, because even if we had assumed some such expressions for the heating/cooling, any attempt to find solutions to the highly nonlinear set of the coupled Eqs. (2.1) would constitute a rather formidable mathematical task. In order to make some progress then, the usual route followed so far has been to replace in the set of the MHD system the energy equation with a polytropic equation of state between the gas pressure and density, $P \propto \rho^\gamma$, for same constant index γ. In this classical polytropic treatment, the distribution of the heating/cooling rate is determined *a posteriori* (Tsinganos et al 1992). However, it is well known by now (Parker 1963) that a

polytropic equation of state with *any* constant value of γ cannot yield correct values of the physical parameters for the best studied outflow, i.e., the solar wind, both close to the Sun and at 1 AU. Also, since such *a priori* specification of a constant γ may correspond to quite artificial heating/cooling distributions along the flow, as well as on streamline shape, we shall follow here a different approach, i.e., we shall restrict our efforts to finding a solution of the dynamical equations (2.1) and then deduce from energy conservation the heating/cooling required to support such a flow pattern. The resulting value of the effective variable γ and the heating distribution can be then regarded as a test of the validity of the specific solution.

Under axisymmetry conditions (i.e., $\partial/\partial\phi = 0$) the poloidal components of the velocity and magnetic field $\mathbf{B}_p$ and $\mathbf{v}_p$ can be defined through the magnetic flux function $A(r,\theta)$ and the mass flux function $\Psi(r,\theta)$ (for details see Tsinganos 1982, Heyvaerts & Norman 1989):

$$\mathbf{B}_p = \frac{\boldsymbol{\nabla} A}{r\sin\theta} \times \mathbf{e}_\phi \,, \qquad 4\pi\rho\mathbf{v}_p = \frac{\boldsymbol{\nabla}\Psi}{r\sin\theta} \times \mathbf{e}_\phi \,. \tag{2.2a}$$

These equations imply that $\Psi = \Psi(A)$ such that $\mathbf{B}_p$ and $\mathbf{v}_p$ are parallel,

$$\mathbf{v}_p = \frac{\Psi_A}{4\pi\rho}\mathbf{B}_p \,, \tag{2.2b}$$

where $\Psi_A = \mathrm{d}\Psi/\mathrm{d}A$.

The $\phi-$ components of the induction and momentum equations (2.1) can be integrated yielding the following expressions for the toroidal velocity and magnetic field (see e.g. Trussoni et al. 1996):

$$B_\phi = -\frac{L(A)\Psi_A}{r\sin\theta}\frac{1 - r^2\sin^2\theta\,\Omega(A)/L(A)}{1-M^2} \,,$$

$$v_\phi = \frac{L(A)}{r\sin\theta}\frac{r^2\sin^2\theta\,\Omega(A)/L(A) - M^2}{1-M^2} \,, \tag{2.3}$$

where we have defined the poloidal Alfvén number:

$$M^2 = 4\pi\rho\frac{v_p^2}{B_p^2} = \frac{\Psi_A^2}{4\pi\rho} \,. \tag{2.4}$$

The quantity $L(A)$ is the *total* angular momentum carried by the flow along a given streamline A = const., while $\Omega(A)$ is the angular velocity of this streamline at the base of the flow. Regularity conditions in Eqs. (2.3) imply that $L(A)$ and $\Omega(A)$ are not independent: for $M = 1$, we must have $\varpi_*^2(A) = (r_*\sin\theta_*)^2 = L/\Omega$, where ϖ_* is the cylindrical distance of the Alfvén surface ($M = 1$) from the field/flow axis, on each magnetic surface $A = const.$

2.1. Meridionally self-similar scaling laws for the variables

Normalizations. It is convenient to define a reference radius r_o to which all variables will be normalized. In TT91 and TT93, r_o was chosen as the radius of the central body. In the present case conversely it will be assumed that $r_o \equiv r_*$, as in ST94, so that all quantities will be normalized to their values at this Alfvén radius along the polar axis. In particular we define:

$$R = \frac{r}{r_*} \,, \qquad v_*^2 = \frac{B_*^2}{4\pi\rho_*} \,, \qquad \alpha(R,\theta) = \frac{2}{r_*^2 B_*}A(r,\theta) \,,$$

where B_*, v_* and ρ_* are the poloidal magnetic field, velocity and the density on the rotational axis at the Alfvén radius r_*, respectively, while α is the dimensionless magnetic flux function.

Magnetic flux function. The first step in the self-similar technique is to express the magnetic flux function α as a product of functions of its two variables r and θ. Second, we assume that there is a sinusoidal dependence with the colatitude such that the poloidal magnetic field has the angular dependence of a dipole,

$$\alpha(R,\theta) = f(R)\sin^2\theta \,. \tag{2.5}$$

Since on each fieldline (with $\mathbf{B}_p \parallel \mathbf{v}_p$ the definitions "streamline" and "fieldline" are equivalent in the poloidal plane) $\alpha(R,\theta)$ = const, it turns out from Eq. (2.5) that the value of α monotonically increases for the streamlines with increasing distance from the rotational axis (where $\alpha = 0$).

Alfvén surface and density distribution. Third, the Alfvén surface is assumed spherical, $M(R,\theta) = M(R)$. This automatically implies that the density can be expressed in a separable form (see Eq. 2.4), $\rho(R,\alpha) = \Psi_A^2(\alpha)/4\pi M^2(R)$. Expanding $\Psi_A^2(\alpha)$ as a series truncated at its first order, $\Psi_A^2 \propto 1 + \delta\alpha$, the assumption of spherical Alfvén surfaces is equivalent with the following expression for the density,

$$\rho(r,\alpha) = \frac{\rho_*}{M^2(R)}(1+\delta\alpha) \,, \tag{2.6}$$

where the parameter δ controls the non spherically symmetric distribution of the density; for $\delta > 0$ ($\delta < 0$) the density increases (decreases) as we move away from the rotation axis.

Poloidal and toroidal velocity and magnetic field. From the conservation of the mass and magnetic fluxes, taking into account Eqs. (2.2b) and (2.6) we get the following expressions for the two components of the poloidal velocity and magnetic field:

$$v_r = v_* M^2(R)\frac{f(R)}{R^2}\frac{\cos\theta}{(1+\delta\alpha)^{1/2}} \,,$$

$$v_\theta = -v_*\frac{M^2(R)}{2\,R}\frac{\mathrm{d}f(R)}{\mathrm{d}R}\frac{\sin\theta}{(1+\delta\alpha)^{1/2}} \,,$$

$$B_r = B_*\frac{f(R)}{R^2}\cos\theta \,, \qquad B_\theta = -B_*\frac{1}{2R^2}\frac{\mathrm{d}f(R)}{\mathrm{d}R}\sin\theta \,. \tag{2.7}$$

On the other hand, for the toroidal velocity and magnetic field, the following expressions are deduced from Eqs. (2.3), by assuming in addition that the poloidal current along the magnetic and rotational axis is proportional to the magnetic flux function A (ST94, Trussoni et al. 1996):

$$v_\phi = v_*\lambda\frac{f(R)}{R^2}\frac{R^2/f(R) - M^2(R)}{1-M^2(R)}\frac{R\sin\theta}{(1+\delta\alpha)^{1/2}} \,,$$

$$B_\phi = -B_* \lambda \frac{f(R)}{R^2} \frac{1 - R^2/f(R)}{1 - M^2(R)} R \sin\theta \,, \tag{2.8}$$

where the parameter λ is related to the angular velocity of the footpoints of the streamlines at $R = 1$.

Gas pressure. The gas pressure is given as the sum of two terms: one is a function of the coordinate R only (spherically symmetric) while the other depends on both coordinates and has the same expression as the magnetic flux function (Eq. 2.5):

$$P(R, \alpha) = \frac{1}{2} \rho_* V_*^2 [Q_o(R) + Q_1(R) \sin^2\theta] \,. \tag{2.9}$$

A consequence of Eq. (2.9) is that no explicit relation between the density and the pressure of the gas exists, as in the usual polytropic approximation. Alternatively, we can say that the polytropic index γ is not constant but depends on the position along the flow.

The physical implications of the previous assumptions for the resulting expressions of the angular momentum loss rate, mass flux, net heating and electric current density distributions are discussed in detail in ST94.

2.2. Equations for the outflow

Following the previous assumptions, Eqs. (2.1) can be rearranged as a system of three ordinary equations in R for the four variables $M(R)$, $f(R)$, $Q_o(R)$ and $Q_1(R)$. At this point a final choice is necessary for the variable Q_1. If we assume $Q_1 \propto Q_o$ the three unknown variables are M, f and Q_o and hence the structure of the streamlines can be deduced. We will call this class of solutions as *free* streamlines case and it was analyzed in detail in ST94 for the particular case of a spherically symmetric distribution of the pressure ($Q_1 = 0$).

If on the other hand, the terms Q_o and Q_1 are kept unrelated, as in the present study, the function $f(R)$ must be prescribed, and the unknown variables are then $M(R)$, $Q_o(R)$ and $Q_1(R)$. This class of solutions (that we shall call *prescribed* streamlines case) can be considered complementary with respect to the *free* streamlines case. Both cases allow to study the physical properties of a fully anisotropic wind with different degrees of collimation.

Taking into account these remarks, from the θ- and r-components of the momentum conservation law (Eq. 2.1) we obtain the following system of equations:

$$\frac{f f'}{2R^2} \frac{\mathrm{d}M^2}{\mathrm{d}R} = Q_1 + \frac{f}{2R^2} \left(f'' - \frac{2f}{R^2} \right) - \frac{M^2}{2R^2} \left[f f'' - \frac{(f')^2}{2} \right]$$

$$- \frac{\lambda^2}{(1 - M^2)^2 R^2} \left[\frac{1}{M^2} (f M^2 - R^2)^2 - 2(f - R^2)^2 \right] \,, \tag{2.10a}$$

$$\frac{\mathrm{d}Q_1}{\mathrm{d}R} = \frac{2f^2}{R^4} \frac{\mathrm{d}M^2}{\mathrm{d}R} - \frac{\delta \nu^2}{M^2 R^2} f - \frac{f'}{2R^2} \left(f'' - \frac{2f}{R^2} \right)$$

$$+ \frac{M^2}{R^3} \left[\frac{(f')^2}{2} - \frac{4f^2}{R^2} + \frac{f f'}{R} \right]$$

$$+ \frac{2\lambda^2}{R^2 (1 - M^2)} \left[\frac{1}{M^2 R} \frac{(M^2 f - R^2)^2}{1 - M^2} \right.$$

$$\left. - (f - R^2) \frac{\mathrm{d}}{\mathrm{d}R} \left(\frac{f - R^2}{1 - M^2} \right) \right] \,, \tag{2.10b}$$

$$\frac{\mathrm{d}Q_o}{\mathrm{d}R} = - \frac{2f}{R^2} \left[\frac{f}{R^2} \frac{\mathrm{d}M^2}{\mathrm{d}R} + \frac{M^2}{R^2} \left(f' - \frac{2f}{R} \right) \right] - \frac{\nu^2}{M^2 R^2} \,, \tag{2.10c}$$

where with primes we indicate the derivatives with respect to R, and have defined $\nu^2 = V_{esc}^2 / v_*^2 = 2\mathscr{G} m / r_* v_*^2$.

If the poloidal streamlines are assumed radial everywhere ($f = 1$), Q_o is given by Eq. (2.10c) while M^2 by Eq. (2.10b) which now becomes:

$$\frac{\mathrm{d}M^2}{\mathrm{d}R} = \left[\frac{\delta \nu^2}{M^2} - \frac{4}{R^3} (1 - M^2) + \frac{4}{R} \frac{\lambda^2}{(1 - M^2)} \right]$$

$$\times \left[\frac{2}{R^2} - \frac{\lambda^2}{(1 - M^2)} \left(\frac{2M^2 - 1}{M^4} R^4 - 1 \right) \right]^{-1} \,. \tag{2.10d}$$

Finally, from Eq. (2.10a) we have the following analytical expression for Q_1:

$$Q_1 = \frac{1}{R^4}$$

$$+ \frac{\lambda^2}{(1 - M^2)^2 R^2} \left[\frac{1}{M^2} (M^2 - R^2)^2 - 2(1 - R^2)^2 \right] \,. \tag{2.10e}$$

These two last equations coincide with Eqs. (2.20) and (2.23) of TT91, apart from the different normalization and the change of variable $v_r \to M^2$ (see also Tsinganos et al. 1992).

2.3. Prescription of the streamline pattern

Similarly to our previous studies in TT91 and TT93, the following simple expression will be assumed for the poloidal streamline shape. Such a shape allows to describe most of the possible geometries of axisymmetric outflows,

$$f(R) = \frac{1 + a R^n + b R^{-m}}{1 + a + b} \,, \tag{2.11}$$

with n, m, a and b nonnegative constants. We recall that for $a = b = 0$ the poloidal fieldlines are radial, as analyzed in TT91, while for $a = 0$ and $b \neq 0$ the streamlines converge initially towards the equatorial plane while asymptotically they become radial (see Low & Tsinganos 1986, Tsinganos & Low 1989).

In the general case with a and b non zero, the streamlines expand towards the equatorial plane in the inner zone, before they converge towards the axis asymptotically. The particular value $n = 2$ corresponds to streamlines which collimate asymptotically to cylinders, a configuration studied in TT93 for the nonrotating case. Note the inflection point of the fieldlines at $R_i = (m\,b/n a)^{1/n+m}$ and also a separatrix value θ_M of the colatitude at the Alfvén point, separating two different regimes. In the inner region of the jet, between the flow axis, $\theta = 0$, and $\theta = \theta_M$, the streamlines are open and rooted to the central body.

On the other hand, if $R_i > 1$, for $\theta > \theta_M$ the fieldlines are closed creating a dead zone without flows around the equator of the central body (Mestel 1968), while if $R_i < 1$ at $\theta > \theta_M$ the fieldlines are rooted vertically to an accretion disk at $\theta = 90^o$ which may orbit around the spherical body. The separatrix value θ_M is,

$$\theta_M = \sin^{-1}\left[\frac{1+d}{1+a+b}\right]^{1/2},$$

$$d = \left(1+\frac{m}{n}\right)\left(\frac{n^m a^m b^n}{m^m}\right)^{\frac{1}{n+m}}. \quad (2.12)$$

A typical pattern of such poloidal streamlines is shown in Fig. 1 of TT93.

For monotonically focused flows, $b = 0$, as the outermost streamline rooted on the central body may be taken that one which emerges with $\theta = 90^o$ at the base of the wind R_o, where $M_o \approx 0$. This same streamline makes an angle θ_{out} at the Alfvén surface :

$$\theta_{out} = \sin^{-1}\left[\frac{1+aR_o^n}{1+a}\right]^{1/2}, \quad (2.13)$$

with the value of R_o given by the complete solution. We expect a strong initial expansion of the wind ($a \ll 1$) and the Alfvén radius to be large compared with the stellar radius to have an efficient magnetic lever arm, such that usually $aR_o^n \ll 1$. As a consequence, all fieldlines cross the Alfvén surface with colatitudes $\theta \leq \theta_{out} \sim \sin^{-1}[1/(1+a)]^{1/2}$. The streamlines with $\theta \geq \theta_{out}$ are not connected to the central body but to the disk orbiting around it.

It is clear from Eq. (2.11) that the values of the parameters a and b rule the basic structure of the streamline system. First, the quantity $R_c \equiv a^{-1/n}$ is a measure of the collimation distance such that for small values of a the flow is focused far from the Alfvén distance, while for $a \sim 1$ collimation is already achieved at the Alfvén distance. Second, the larger is b, the more "open" the fieldlines are before reaching their asymptotic width. This behavior can be easily seen by introducing the function $G(R) = R/\sqrt{f}$ defined in ST94, which gives the transverse width of the flow channel normalized in units of its width at $R = 1$. For cylindrical collimation ($n = 2$) in the asymptotic region ($R \gg 1$) the normalized width of the channel is given by $G_\infty = \sqrt{(1+a+b)/a}$. It is evident thence that the closer is the collimation distance to the Alfvén point (large values of a) the narrower is the jet, while small values of a and a "flaring" of the fieldlines in the inner region ($b \neq 0$) lead to wider beams. Actually, we shall see in the following that the asymptotic speed of the flow is directly related to these streamline parameters.

2.4. Singularities of the equations and boundary conditions

Before we proceed with a presentation of the solutions of Eqs. (2.10), we briefly point out some differences with respect to the analysis of ST94 for the case of free streamlines. First of all, we deal here with a system of three first order differential equations, while in ST94 the equations are four, with $G(R)$ defined as the fourth unknown. Also, in Eqs. (2.10a) and (2.10b) Q_o is not appearing, so that Eq. (2.10c) is decoupled from the other two equations. In general this is not the case for the free streamlines model, unless the pressure is assumed spherically symmetric, as in ST94 wherein $Q_1 = 0$. On the other hand, a rather crucial difference is that in the free fieldlines case an actual integral of the motion exists, related to the difference of energy along the rotational axis and the other streamlines without any such equivalent integral in the present prescribed streamlines case. Furthermore, the topological structure of the solutions is also different in the two sets of equations. Thus, apart from the usual presence of a singularity at the Alfvén point ($f = R = M = 1$) in both cases, in ST94 an X–type critical point is also present. We should note that no such critical point appears in our case for $n \neq 0$, although various other singularities are present, as we shall discuss below.

Alfvén singularity. To solve the equations close to the Alfvén transition we follow the same procedure as in ST94. *First*, the toroidal velocity and magnetic field at $R = 1$ are given in terms of the slope of M^2 at the Alfvén point, $(\mathrm{d}M^2/\mathrm{d}R)_{R=1} \equiv p$ and the streamline constants (n, m, a, b),

$$\lim_{R\to 1}\left[\frac{f-R^2}{1-M^2}\right] = \frac{2-f'_*}{p}, \quad (2.14a)$$

$$\lim_{R\to 1}\left[\frac{fM^2-R^2}{1-M^2}\right] = \frac{2-f'_*}{p} - 1, \quad (2.14b)$$

where

$$f'_* = \frac{1+na-mb}{1+a+b}. \quad (2.14c)$$

And *second*, the Alfvén regularity condition in Eq. (2.10a) gives the following third degree polynomial for p at $R = 1$,

$$\frac{f'_*}{2\lambda^2}p^3 + \left[1-\frac{1}{\lambda^2}\left(Q_1^* + \frac{(f'_*)^2}{4} - 1\right)\right]p^2$$

$$-2(2-f'_*)p - (2-f'_*)^2 = 0. \quad (2.15)$$

It follows that the Alfvén regularity condition relates the slope p of the square of the Alfvén number at the Alfvén point to the streamline constants, f'_*, as well as to the magnitude of rotation λ and the anisotropic pressure component Q_1^*. Note that a cubic relation similar to Eq. (2.15) is obtained by Heyvaerts & Norman (1989) and also by ST94 for the case of free streamlines. Apparently, for $0 \leq n \leq 2$ and $m > 0$, we need to consider only real and positive roots of Eq. (2.15) for typical outflow solutions.

"Flexus" singularity. It is evident from Eqs. (2.10a) and (2.11) that when $b \neq 0$, a singularity may be present at $R = R_i$, where the streamlines have a flexus and the velocity along the self-similarity direction θ vanishes, $f'(R_i) = 0$. This singularity appears also in nonrotating flows (see TT93). However, R_i is not a true critical point and the streamlines become simply locally

radial there while the system lowers from the second to the first order. Accordingly, Eqs. (2.10a) and (2.10b) become very similar to Eqs. (2.10d) and (2.10e), with some extra terms proportional to the θ components of the inertial forces and the gradient of the magnetic fields. These components are proportional to $\partial B_\theta/\partial R|_{R=R_i}$ and $\partial v_\theta/\partial R|_{R=R_i}$ which are not vanishing even though $v_\theta(R = R_i) = B_\theta(R = R_i) = 0$.

Asymptotic singularity. Although no other singularity appears explicitly in Eqs. (2.10) at a finite distance R, we already know from the nonrotating case that as $R \to \infty$ the equations become extremely stiff (see TT93). Indeed, the same behaviour is found in the present case for $R \gg 1$. The topologies become similar to those in the region upwind of a classical "X-type" critical point, i.e., it appears that a critical point is present at infinity. This behaviour has been also found in winds with different acceleration processes (e.g., winds driven by heat conduction, Weber 1970, or radiativelly driven winds, Żytkow 1972).

The topologies are completely different from those found for radial outflows ($f = 1$), in which case an X-type critical point appears at a *finite* radial distance for $R > 1$ (see TT91). From the mathematical point of view we can consider the radial configuration as a degenerate case of the general one in the limit of a, $b \to 0$, with the system of equations switching from the second order (Eqs. 2.10a–c) to the first order (Eq. 2.10d).

We must remark now that our topologies are quite different from those found by Rotstein & Ferro Fontán (1995a) for the case of rotating flows which are loosely collimated. In fact their solutions show an X-type critical point downstream of the Alfvén surface, similarily to TT91. It is not clear however whether this is due to an approximate treatment of the equations in the superAlfvénic region, or to the assumed logarithmic streamline shape.

Boundary conditions. The topologies of the 2-D MHD equations are quite complicated (see e.g. ST94), so we will discuss here only their main features, starting from the behaviour of the solutions close to the Alfvén point.

For $R = 1$ the value of M is fixed to 1 by our assumed normalization, so the topologies for a given streamline shape (m, n, a, b) and rotation constant λ are ruled only by the value of Q_1^*, which determines the slope of M^2 at $R = 1$. For the case of radial streamlines ($f' = 0$, studied in TT91) Eq. (2.15) reduces to a second degree polynomial, with the positive root (provided that $Q_1^* < 1 + 2\lambda^2$):

$$p = \frac{2\lambda}{\sqrt{2\lambda^2 + 1 - Q_1^*} - \lambda}\,. \tag{2.16}$$

It maybe worth to emphasize for a moment the peculiarity of this case with radial streamlines and also compare it to the classical 1-D case of Weber & Davis (1967). *First*, note that, although in Eq. (2.10d) the slope p of M^2 does not depend explicitly on Q_1^*, this parameter Q_1^* is indeed related to p through the analytical expression of Eq. (2.10e), i.e., Q_1^* and p are finally interelated, as shown by Eq. (2.16). *Second*, the solution topologies in the $(M^2,\ R)$ plane are very similar to those obtained in the 1-D case of Weber & Davis (1967), with a single X-type critical point in the downstream region (see Figs. 5 of TT91). However, it must be taken into account that in the 1-D geometry the transfield equation is not considered at all, such that the Alfvèn singularity is not a critical point, in agreement with the general properties of MHD axisymmetric winds (for details see Tsinganos et al. 1996). *Third*, although the solution is selected by the critical point downstream of the Alfvèn singularity as in the Weber & Davis (1967) case, now the transfield equation is included, Eq. (2.10e). This appears from the fact that at each slope at $R = 1$ correspond different values of the pressure (see Eq. 2.16), contrary to the 1-D polytropic case, even though the topologies are very similar. In other words, for each solution that appears as a star-like point across the Alfvén surface exists only a unique value of the pressure through Eq. (2.16), contrarily to the Weber & Davis' topology.

For $n > 0$ the situation changes drastically as the critical point is ejected to infinity. Q_1^* is then given by the differential Eq. (2.10b) while it also appears explicitly in the equations for M^2. Therefore in such a case the topologies are accordingly different. In particular, there exists a value $Q_{1,s}^*$ that selects two different groups of solutions. For $Q_1^* > Q_{1,s}^*$ we have $\mathrm{d}M^2/\mathrm{d}R \to \infty$ such that both M and Q_1 diverge asymptotically. For $Q_1^* < Q_{1,s}^*$ conversely the topological behaviour depends on the value of n. For $n < 2$, Q_1 drops fast to negative values and M becomes very small. For $n = 2$, M and the quantity Q_1/R^2 converge to finite values such that the smaller is Q_1^* the smaller is also the asymptotical value of M (for details see next section). We remark here that the situation is analoguous to chaotic dynamical systems which are extremely sensitive to the initial conditions (Baker & Gollub 1990). Here, small changes in the conditions at the Alfvén point (value of Q_1^*) lead to widely different final solutions.

From these considerations we can fix the boundary conditions of the problem. At $R = 1$ we automatically have $M = 1$ while, in order to have a regular solution at infinity, a value of $Q_1^* = Q_{1,s}^*$ must be selected, apart the fully collimated case for which solutions with $Q_1^* < Q_{1,s}^*$ are also allowed (this point will be discussed in more detail in Sec. 4). In the case of expanding streamlines, $n < 2$, the value of Q_o at $R = 1$ (Q_o^*) must be selected such that the total pressure vanishes at $R \to \infty$ and is positive all along the flow. For $n = 2$ conversely the asymptotic pressure can converge to a constant value, so that a range of values of Q_o^* can be chosen.

3. Asymptotic analysis

Analytical results from Eqs. (2.10) can be obtained in the sub-Alfvénic region close to the base of the flow by assuming $b = 0$, and in the superAlfvénic region, for cylindrical collimation ($n = 2$).

3.1. SubAlfvénic accelerating flow: R, $M \ll 1$

We can perform a simple asymptotic analysis of the flow in the subAlfvénic region if the streamlines are monotonically focusing polewards ($b = 0$). Then, close to the base the poloidal

streamlines become basically radial for $R \ll R_c = 1/\sqrt{a}$ (see Eq. 2.11). Therefore in this radial region the dynamics of the wind can be described by Eq. (2.10d) which becomes, for $M_o \lesssim M \ll 1$ and $R_o \lesssim R \ll 1$:

$$\frac{\mathrm{d}M^2}{\mathrm{d}R} = \left[\frac{\delta\nu^2}{M^2} - \frac{4}{R^3}(1-\lambda^2R^2)\right] \times \left[\frac{2}{R^2} + \lambda^2\left(\frac{R^4}{M^4}+1\right)\right]^{-1} . \quad (3.1)$$

From this expression the following trends are evident. First, if $\delta\nu^2 = \lambda^2 = 0$ we have $\mathrm{d}M^2/\mathrm{d}R < 0$. In other words, there is no acceleration in a magnetized but *nonrotating* flow with a *spherically* symmetric density distribution, as already discussed in TT93.

Second, consider the acceleration at the base of the wind [$R = R_o(1+\epsilon)$, $\epsilon \ll 1$] in the case wherein $\delta\nu^2 \neq 0$ and $\lambda^2 \neq 0$. From Eq. (3.1) we see that we do get an acceleration [a positive slope of $M^2(R)$] only when $\delta\nu^2 > (\delta\nu^2)_o \equiv 4M_o^2/R_o^3(1-\lambda^2R_o^2)$ [see also Eq. (5.1a) in TT91]. This means that there is a lower limit $(\delta\nu^2)_o$ in order to have accelerating outflow solutions close to the base; this limit decreases by increasing the rotation parameter λ. Also, the initial acceleration rate increases with $\delta\nu^2$ and reduces by increasing the rotation parameter λ.

In conclusion, the flow at its base is mainly thermally driven and its dynamics is strictly dependent on the anisotropic distribution of the density and on the gravitational field of the central body. This dependence of the acceleration on $\delta\nu^2$ can be explained as follows. A dipolar magnetic field needs to be kept open by a pressure that must decrease towards the pole. With a density which does not decrease with latitude sufficiently fast [$\delta\nu^2 < (\delta\nu^2)_o$], there is a smaller pressure gradient to drive the flow near the pole, exactly where the magnetic field is open to allow the wind to escape. The resulting acceleration is too low, since gravity dominates, and the flow does not reach a high enough terminal speed. The only way out is to allow density to decrease with latitude sufficiently fast (faster than the pressure does), i.e. $\delta\nu^2 > (\delta\nu^2)_o$ (Hu & Low 1989).

3.2. SuperAlfvénic collimated flow: $R \gg 1$, $n = 2$

In the asymptotic region ($R \gg 1$) the cylindrically collimated outflow attains a configuration with constant cross sectional area and Alfvén number. As $(\mathrm{d}M^2/\mathrm{d}R)_{R\to\infty} = 0$ in Eq. (2.10a) we obtain the following relation between Q_1 and M_∞:

$$Q_1 = \frac{\lambda^2R^2}{(1-M_\infty^2)^2(1+a+b)^2} \times \left[\frac{a^2}{M_\infty^2}\left(\frac{1+a+b}{a} - M_\infty^2\right)^2 - 2(1+b)^2\right] . \quad (3.2)$$

This expression simply represents force balance in a direction perpendicular to the flow axis: the outwards directed centrifugal force is balanced by the inwards tension of the toroidal magnetic field and gradient of the magnetic pressure, enhanced (reduced) by the gradient of the gas pressure for $Q_1 > 0$ ($Q_1 < 0$),

$$\frac{\rho v_\phi^2}{\varpi} = \frac{\mathrm{d}}{\mathrm{d}\varpi}\left[\frac{B_\phi^2}{8\pi} + P\right] + \frac{B_\phi^2}{4\pi\varpi} , \quad (3.3)$$

where $\varpi = r\sin\theta$. For $Q_1 = 0$, i.e. if there is no pressure to confine the jet asymptotically, Eq. (3.2) reduces to

$$\left(\frac{1+a+b}{a} - M_\infty^2\right)^2 = 2\left(\frac{1+b}{a}\right)^2 M_\infty^2 . \quad (3.4)$$

Force balance across the jet is simply due to the centrifugal force and the magnetic pinching forces. For $a,\ b \ll 1$ (i.e. for large widths of the flow channel), the asymptotic Alfvén number is simply $M_\infty \approx \sqrt{2}/a$ and the cross sectional area $G_\infty^2 = (1+a+b)/a \approx 1/a$, such that the wider is the beam (small values of a, b) the higher is its terminal speed ($V_\infty \propto M_\infty^2/G_\infty^2 \propto 1/a$). As the beam is wider, the conversion of Poynting flux into kinetic energy is more efficient leading to a higher acceleration downstream of the Alfvén surface, and consequently to higher terminal velocities.

By defining the quantity $q = Q_1/R^2\lambda^2$, Eq. (3.2) can be written as a third degree polynomial for M_∞^2:

$$M_\infty^6 - \left[2 + \frac{a^2}{q(1+a+b)^2}\right] M_\infty^4$$

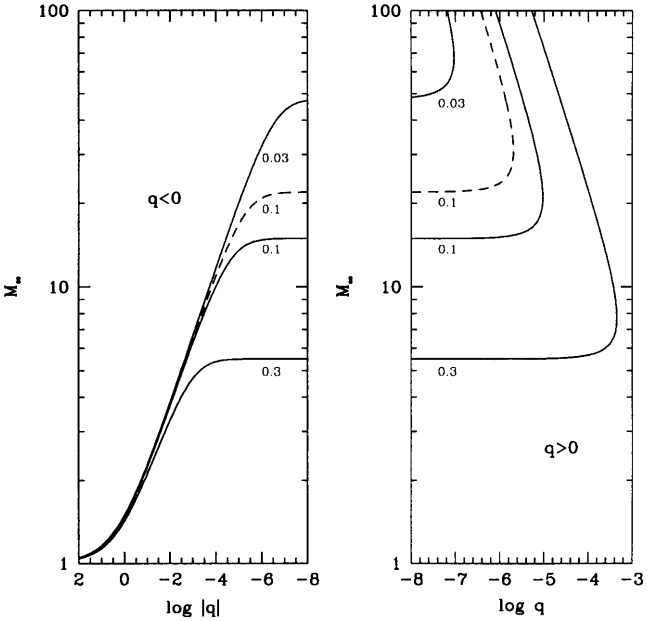

Fig. 1. Plots of the asymptotic Alfvén number M_∞ *vs.* the thermal pressure parameter q, for indicated on the curves values of a. The left panel corresponds to $q < 0$ (overpressured jet) while the right panel to $q > 0$ (underpressured jet). It has been assumed $b = 0$ (i.e. monotonically polewards converging streamlines, see Eq. 2.11) except on the dashed line, where $b = 0.5$ and $m = 1$. The jet is magnetically confined for $q < 0$ and in the lower branches of $q > 0$, while in the upper branches of $q > 0$ the jet is thermally confined.

$$+\left\{1+\frac{2}{q(1+a+b)}\left[a+\frac{(1+b)^2}{1+a+b}\right]\right\}M_\infty^2-\frac{1}{q}=0\,, \quad (3.5)$$

whose real and positive roots provide the asymptotic Alfvén number as a function of the parameters q, a and b. As expected, M_∞^2 does not depend on δ and ν, which govern the wind dynamics only close to the inner part of the flow.

From the plots of M_∞^2 vs q shown in Fig. 1 we note the following basic features. For $q<0$, M_∞ increases by decreasing $|q|$, converging to the value given by Eq. (3.4) for $q=0$. For $q>0$ there are two branches of solutions: the lower one, with M_∞ almost constant, is the extension to positive values of q of the previous solution, while the upper branch, with much higher values of M_∞^2, diverges for $q\to 0$. These two branches merge at an upper limit of q, $q=q_{max}$, and for $q>q_{max}$ no collimated solutions are found. Accordingly, the value of q_{max} can be considered as an upper limit for q_s (where we have defined $q_s=Q_{1,s}/R^2\lambda^2$ and $Q_{1,s}$ is the upper limit above which the solution has an asymptotically diverging pressure; see end of Sect. 2).

We note also that with $b\neq 0$ there is a rapid expansion of the streamlines in the transAlfvénic region, so that the collimated beam is wider. Therefore, for the asymptotic structure of the wind a larger value of b is equivalent to a lower value of a.

These results can be interpreted by writing the force balance, Eq. (3.3), in the following form:

$$F_C-F_B=F_{\nabla P}\,,$$

$$\frac{1}{G_\infty^4M_\infty^2}\left(\frac{G_\infty^2-M_\infty^2}{1-M_\infty^2}\right)^2-\frac{2}{G_\infty^4}\left(\frac{1-G_\infty^2}{1-M_\infty^2}\right)^2=q\,, \quad (3.3')$$

where the first and second member on the left hand side are the centrifugal (F_C) and magnetic stress forces (F_B), while the right hand side is due to the gradient of the gas pressure $F_{\nabla P}$.

From Eq. (3.3') we note that if $M_\infty^2\gg G_\infty^2$, the magnetic stress decreases with M_∞^2 while it is practically unaffected by the width G_∞^2 of the channel. This is well understood if we recall that for $M_\infty^2\to\infty$ we move into the hydrodynamic limit, wherein the magnetic forces vanish and the centrifugal force is balanced by the gas pressure gradient. The centrifugal force conversely decreases both with M_∞^2 (but at a slower rate than F_B) and the beam width. This is consistent with the behaviour of the density, which decreases as $\propto 1/M_\infty^2$, and the rotational velocity, which depends only on the fieldline pattern (see Eqs. 2.6, 2.8a).

For $q=0$ the magnetic pinching force F_B (directed inwards) is exactly balanced by F_C. If we increase M_∞^2, both F_C and F_B decrease, but the later decreases faster: the only way to keep the balance is to further reduce F_C by enlarging the beam width. If $q<0$ a similar argument holds: the gradient of the gas pressure "helps" the centrifugal force to balance the magnetic stress. To maintain the force balance with a kept fixed, F_B must increase by lowering the Alfvén number, and the contribution of F_C with respect to $F_{\nabla P}$ becomes negligible by rising $|q|$ (see Fig. 2). However for $|q|$ large enough $M_\infty^2\to G_\infty^2$, and the centrifugal force vanishes, while $F_{\nabla P}$ does not depend on

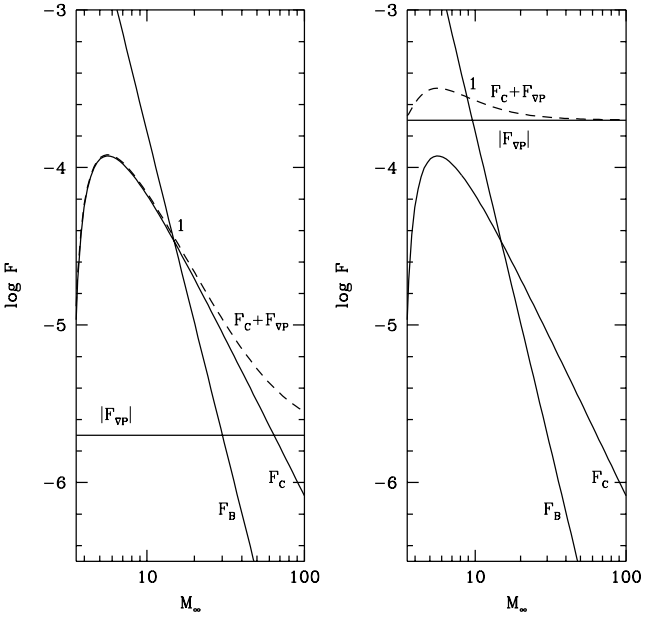

Fig. 2. Plots of the magnitude of the various forces F (F_B, F_C and $F_{\nabla P}$) acting in an overpressured ($q<0$) and collimated jet (in nondimensional units as in Eq. 3.3′) *vs.* the asymptotic Alfvén number M_∞ for $a=0.1$, $q=-2\times10^{-6}$ (left panel) and $q=-2\times10^{-5}$ (right panel). At position 1 we have $F_B=F_C+F_{\nabla P}$ (dashed line): the magnetic pinching force is balanced mainly by the centrifugal force (left panel) or by the pressure gradient (right panel).

M_∞^2. For $M_\infty^2<G_\infty^2$ the magnetic stress is balanced only by the gradient of the gas pressure. It must be noticed however that if $M_\infty^2<G_\infty^2$, there is a reversal of the rotational velocity between the Alfvén surface and the asymptotic region (Eq. 2.8), where the flow velocity results to be lower than at $R=1$ (because it is proportional to M_∞^2/G_∞^2). These solutions can be considered as unphysical, so that a lower limit must be assumed for q ($q=q_{min}$), corresponding to a value $Q_1^*=Q_{1,min}^*$ on the Alfvén surface.

If $q>0$ the gradient of the gas pressure contributes to pinch the flow with the magnetic stress, and we can see from Eq. (3.3') that equilibrium conditions can be fulfiled in two different regimes (see Fig. 3). For M_∞^2 not too large, we have $F_B\approx F_C$, i.e., the centrifugal force is balanced mainly by the magnetic pinch and the value of M_∞ is given by Eq. (3.4). This regime, corresponding to the lower branch in Fig. 1b, is just the extension to positive values of q of the case with $q<0$ discussed above.

On the other hand, F_B rapidly decreases with M_∞^2, so that for large values of the Alfvén number the centrifugal force is balanced mainly by the gas pressure ($F_C\approx F_{\nabla P}$). We are in the thermally dominated regime, corresponding to the upper branch in Fig. 1b, and we converge to the hydrodynamic limit for $M_\infty\to\infty$. In such a case, from Eq. (3.3') we have $M_\infty^2\approx a^2/q$ and the asymptotic value of the flow speed on the rotational axis is $v_r\propto M_\infty^2/G_\infty^2\propto a^3/q$.

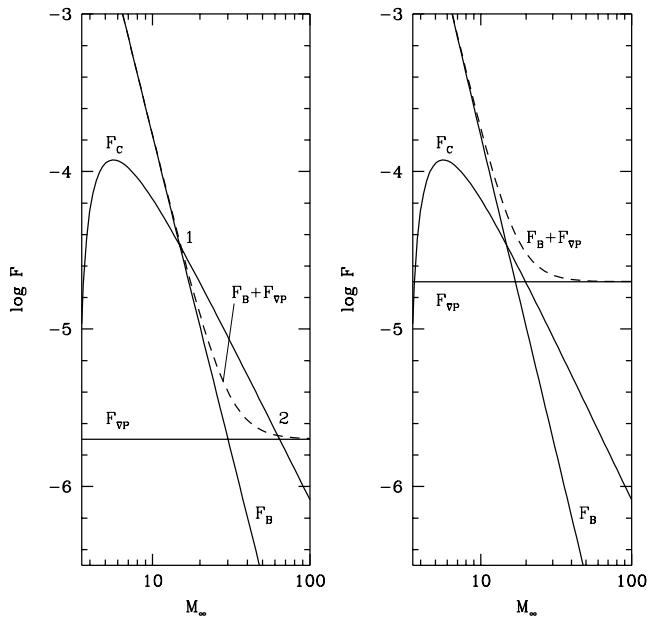

Fig. 3. The same as Fig. 2 for an underpressured jet ($q > 0$): $q = 2 \times 10^{-6}$ (left panel) and $q = 2 \times 10^{-5}$ (right panel). At the intersections 1 and 2 in the left panel is $F_C = F_B + F_{\nabla P}$ (dashed line): the centrifugal force is balanced mainly by the magnetic stress at position 1 ("magnetic regime") and by the pressure gradient at position 2 ("thermal regime"). No equilibrium is attained for the case plotted in the right panel.

We may conclude then, that in the collimated flow dynamics we distinguish a "thermal regime" (upper branch) from a "magnetic regime" (lower branch). These two branches merge at $q = q_{max}$ (with a corresponding value of $Q_1^* = Q_{1,m}^*$ at the Alfvén radius) and no collimated solution exists for $q > q_{max}$. In such a case the pinching forces always prevail and the beam cannot be in equilibrium unless the structure of the streamlines is changed (F_B+$F_{\nabla P} > F_C$, see Fig. 3, right panel). It is therefore worth to point out that if there is no adequate internal thermal pressure to balance the magnetic stresses, the beam may collapse to its axis. This situation might explain why in some magnetically dominated, radially self-similar solutions (Blandford & Payne 1982, Ferreira 1997) the streamlines refocus and cross the flow axis and the equilibrium solution cannot be extended to large distances. In other words, in a magnetically dominated beam adequately high internal thermal pressure is needed at its core to balance the pinching magnetic stresses and if such internal thermal pressures are not available the beam may not find a dynamical equilibrium to extend to infinity. On the other hand, a hydrodynamically dominated beam needs to be underpressured such that the centrifugal forces are balanced by this confining thermal pressure.

Finally, we note that Eq. (3.5) is similar to the corresponding equation obtained in the free streamlines case of ST94 by assuming a spherically symmetric distribution for the pressure. This Eq. (5.11) in ST94 is valid also in the case of nonspherically symmetric pressure distribution, provided that asymptotically the pressure vanishes.

4. Results: numerical solutions

In this section we present the results of the numerical integration of Eqs. (2.10) and provide complete solutions which connect the subAlfvénic and the superAlfvénic regions, for some significant values of the parameters.

Numerical technique. Following the usual procedure, Eqs. (2.10) are integrated upstream and downstream from the Alfvén point, starting from $R = 1 \pm p\,\mathrm{d}R$ (with $\mathrm{d}R \ll R$) using a standard Runge–Kutta algorithm suited for the integration of stiff systems of differential equations. In the upstream region the integration is carried out until a value $R = R_o$ where $M \to 0$ and which will be assumed as the base of the outflow close to the central body.

In the downstream region we cannot follow the same simple technique, because of the presence of the critical point at infinity. With the Runge–Kutta code we first tune as precisely as possible the value of Q_1^* close to $Q_{1,s}^*$, which gives a solution asymptotically regular. Thence (as done also for the nonrotational case in TT93), the solution is refined by means of a finite difference code (Nobili & Turolla 1988). This procedure must be also followed in the case where $n = 2$ for which a range of acceptable solutions exists for $Q_{1,min}^* \le Q_1^* \le Q_{1,s}^*$, as we discussed in the previous section. In fact, it turns out that the two limits $Q_{1,min}^*$ and $Q_{1,s}^*$ are practically coincident.

Choice of the parameters. Referring to the geometrical shape of the streamlines, we concentrate mainly to the case with $b = 0$ and $n = 2$, i.e., streamlines monotonically converging towards the rotational axis and cylindrically collimated for $R \gg 1$. The numerical technique used in the downwind region does not allow to follow the solutions farther than $R_\infty \approx 10^4 - 10^5$. This implies some constraints on the value of a: as the asymptotic region must be attained in the solutions at distances $R < R_\infty$, the width of the beam cannot be too large. In the following, we shall mainly adopt the value $a = 0.1$, which means that asymptotically the collimated streamlines have a radius ≈ 3.2 larger than their value at $R = 1$.

The quantity $\delta\nu^2$ rules the flow acceleration mainly in the subAlfvénic and transAlfvénic region, since asymptotically the flow velocity depends only on the ratio Q_1/λ^2. However, the asymptotic value of Q_1 depends on the value of $\delta\nu^2$ through the integration of Eqs. (2.10). Conversely Q_o depends solely on the value of ν^2.

According to the asymptotic analysis of Sect. 3.1, we shall assume $\delta\nu^2 \ge (\delta\nu^2)_o$ which allows physically acceptable outflow solutions, with $(\delta\nu^2)_o$ depending on λ. The value of λ is fundamental for the wind dynamics since it governs the plasma acceleration at the base and in the asymptotic region. We shall mainly analyze solutions for $\lambda = 0.3$ and $\lambda = 3$, corresponding to the two representative cases of slow and relatively faster rotation.

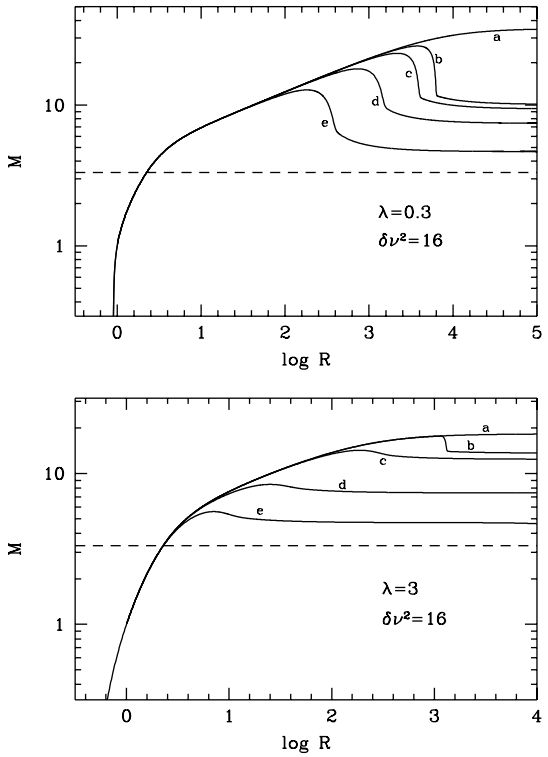

Fig. 4. Plot of M *vs.* the dimensionless radial distance R along the polar axis for $\delta\nu^2 = 16$. *Upper panel*: $\lambda = 0.3$ and $q = 5.6 \times 10^{-6}$ ($\equiv q_s$, a), -9.3×10^{-5} ($\equiv q'$, b), -1.4×10^{-4} (c), -4.6×10^{-4} (d) and -3.7×10^{-3} (e). *Lower panel*: $\lambda = 3$ and $q = 8.3 \times 10^{-6}$ ($\equiv q_s$, a), -8.3×10^{-6} ($\equiv q'$, b), -2.3×10^{-5} (c), -4.6×10^{-4} (d) and -3.7×10^{-3} (e). Plots (b) - (e) are the bumpy solutions, while the dashed line marks the minimum value $M(q = q_{min})$, where $q_{min} = -0.0165$.

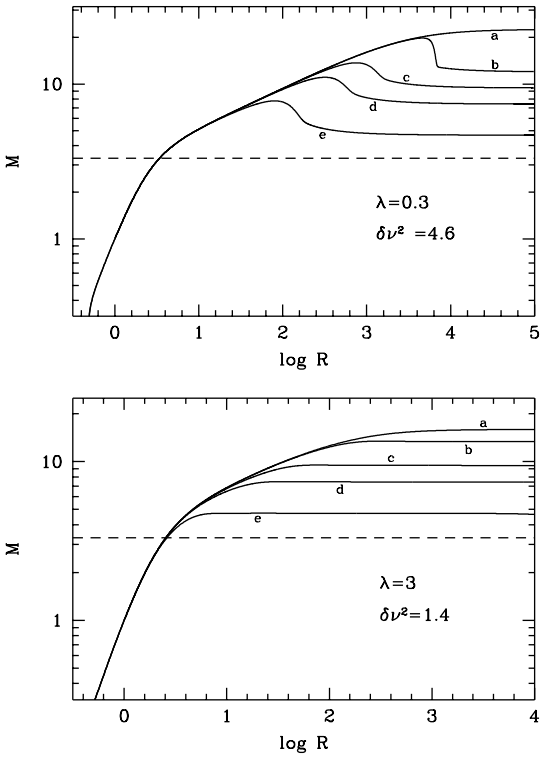

Fig. 5. Plot of M *vs.* the dimensionless radial distance R along the polar axis for $\delta\nu^2 \approx (\delta\nu^2)_o$. *Upper panel*: $\lambda = 0.3$, $\delta\nu^2 = 4.6$ and $q = 9.3 \times 10^{-6}$ ($\equiv q_s$, a), -3.1×10^{-5} ($\equiv q'$, b), -1.4×10^{-4} (c), -4.6×10^{-4} (d) and -3.7×10^{-3} (e). *Lower panel*: $\lambda = 3$, $\delta\nu^2 = 1.4$ and $q = 4.2 \times 10^{-6}$ ($\equiv q_s$, a), -1.1×10^{-5} (b), -1.4×10^{-4} (c), -4.6×10^{-4} (d) and -3.7×10^{-3} (e); the solution with $q = 1.3 \times 10^{-6}$ ($\equiv q'$) is almost overlapping with solution (a).

4.1. Solutions for slowly and fastly rotating outflows

The plots of M *vs.* R along the polar axis ($\alpha = 0$) for $\delta\nu^2 = 16$ [$\gg (\delta\nu^2)_o$] and some values of $q = [Q_1/(R^2\lambda^2)]_\infty$ are shown in Fig. 4 for the two cases of $\lambda = 0.3$ (slower rotation) and $\lambda = 3$ (faster rotation).

From the numerical analysis a different behaviour of the outflow emerges at $R \gg 1$, $R \gtrsim 1$ and $R < 1$. In the subAlfvénic region the acceleration rate is quite large and increases by decreasing λ, as we have seen in Sect. 3.1. As a consequence, the Alfvén radius is closer to the base of the flow the slower is the rotation rate. Thus, we find $R_o = 0.85$ ($\lambda = 0.3$) and $R_o = 0.47$ ($\lambda = 3$), with $\theta_{out} \approx 81^o$ and $\theta_{out} \approx 75^o$, respectively, as values of the colatitude at $R = 1$ for the outermost streamline (see Eq. 2.13).

On the other hand, for $R \gg 1$ the Alfvén number reaches a constant value which lowers by reducing q, as predicted by the analysis of the previous section. In the inner accelerating region, where the flow is subAlfvénic and transAlfvénic, M rapidly increases: the acceleration is practically insensitive to the different values of q and the different solutions overlap. In the transition region between these two regimes, the velocity reaches a maximum ("bump"). The position of this bump shifts outwards by increasing q, while its shape simultaneously steepens up to a rather sharp transition between the inner and the outer part of the outflow. When $q \to q_s$, with q_s defined in Sect. 3.2, the bump disappears and we obtain a solution which is monotonically increasing before reaching its asymptotic value.

It appears however that this monotonically increasing solution cannot be smoothly attained by the "bumpy" solutions by simply increasing Q_1 at the base. In fact, when the transition region is shifted downwind by increasing Q_1 and basically becomes a discontinuity, it reaches a limiting distance, corresponding to a maximum value of q ($\equiv q'$).

From this behaviour we deduce that there are some limits in the values of q and M for which solutions can be obtained. *First*, we have the monotonically increasing solution for $Q_1 = Q_{1,s}$. *Second*, no solution is found for $Q_1 < Q_{1,s}$, corresponding to values of q in the range $q' < q < q_s$. *Third*, by further reducing Q_1 the bumpy solutions are found for corresponding values of q in the interval $q_{min} \leq q \leq q'$.

The above general trends are not qualitatively modified by the value of the rotational velocity. For $\lambda = 0.3$ we find $q_{min} = -1.65 \times 10^{-2}$, $q' = -9.3 \times 10^{-5}$ and $q_s = 5.6 \times 10^{-6}$. It is worth to note that in the monotonically increasing solutions the asymptotic region is reached at $R \approx 3 \times 10^4$, while

it is attained much closer to the Alfvén surface for the bumpy solutions. Furthermore, this asymptotic regime is reached at distances $\gg R_c$, where the streamlines become cylindrically collimated. For $\lambda = 3$ the increase of velocity is slower, as predicted by the analysis in Sect. 3.1, so that the asymptotic Alfvén number in the monotonically increasing solution is reduced. Since in the bumpy solutions the value of M_∞ depends on q only, we have a lowering of the amplitude of the bumps, and their position is shifted upwind by a factor ≈ 10 with respect to solutions with $\lambda = 0.3$. Accordingly, the gap between the bumpy and monotonically increasing solutions is much narrower, with $q' = -8.2 \times 10^{-6}$ and $q_s = 8.3 \times 10^{-6}$.

We can now summarize the general properties of our solutions keeping in mind the asymptotic analysis of Sect. 3.2. *First*, the bumpy solutions found for $q < 0$ are always magnetically confined. *Second*, the monotonically increasing solutions are found for $q > 0$ and the asymptotic analysis predicts that they can be either in the magnetically or in the thermally dominated regime (see Figs. 1 - 3). We can see that for $\lambda = 0.3$ (slow magnetic rotator, SMR), the asymptotic Alfvén number of the monotonically increasing solution attains a value which is on the upper branch (thermally dominated) of Fig. 1, while for $\lambda = 3$ (faster magnetic rotator, FMR) it attains a value which is on the lower branch (magnetically dominated) of Fig. 1. More in general, moving from a SMR to FMR, first q_s increases and the asymptotic value of M rapidly decreases, thence, when $q_s \to q_{max}$ ($q_{max} = 9.4 \times 10^{-6}$ for the assumed parameters), M "turns around" and slowly decreases with q_s.

It is worth to note that the gap between the bumpy and monotonically increasing solutions appears predominantly for the SMR (upper panels of Figs. 4 and 5), in which case the monotonically increasing solution corresponds to a jet basically confined by the thermal pressure gradient. We have seen that for such a solution the value of Q_1 is tuned precisely to Q_{1s}. If Q_1 is slightly lower than Q_{1s}, the final equilibrium cannot be attained and instead there is a jump to lower Mach numbers, that allows the flow to become magnetically confined asymptotically and overpressured ($q \leq q' < 0$). Conversely, in the case of FMR (lower panels of Figs. 4 and 5) the continuous and the bump solutions are both magnetically confined, so the gap and the sharpness of the bump almost disappear.

We remark that the presence of maxima and/or periodic oscillations is a rather general behaviour, which does not appear to be related only to our specific assumptions. Similar results have been also found by Blandford & Payne (1982), Pelletier & Pudritz (1992), ST94. The effect is simply related to the balance of the forces acting on the flow: centrifugal force, magnetic tension and gas pressure gradient. In particular, the oscillations found in ST94 are due to the interplay of the centrifugal force and the toroidal magnetic field, with no effect from the gas pressure gradient since $\kappa = 0$ (i.e., the flow is always magnetically confined). In the present model, conversely, the bump is strictly related to the gradient of the gas pressure.

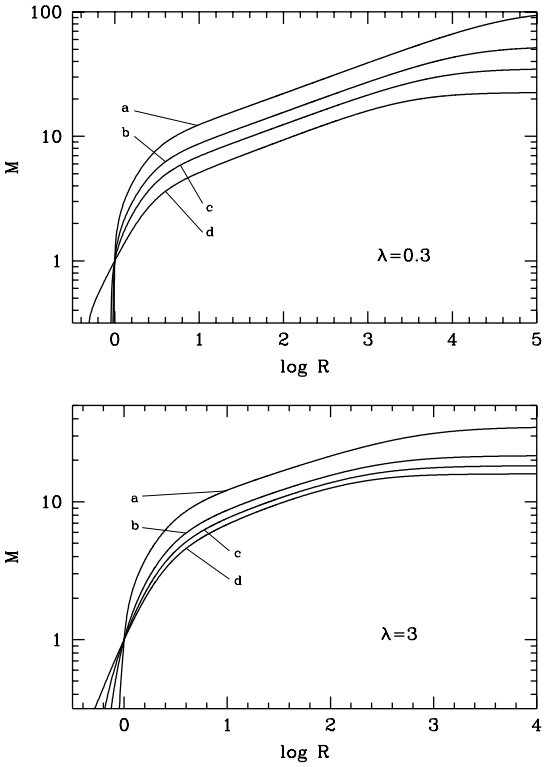

Fig. 6. Plot of M for the monotonically increasing solutions *vs* the dimensionless radial distance R along the polar axis, for different values of $\delta\nu^2$. *Upper panel*: $\lambda = 0.3$ and $\delta\nu^2 = 160$ ($q_s = 9.1 \times 10^{-7}$, a), 40 ($q_s = 2.9 \times 10^{-6}$, b), 16 ($q_s = 5.6 \times 10^{-6}$, c) and 1.4 ($q_s = 9.3 \times 10^{-6}$, d). *Lower panel*: $\lambda = 3$ and $\delta\nu^2 = 160$ ($q_s = 5.6 \times 10^{-6}$, a), 40 ($q_s = 9.3 \times 10^{-6}$, b), 16 ($q_s = 8.3 \times 10^{-6}$, c) and 4.6 ($q_s = 4.2 \times 10^{-6}$, d).

4.2. Effect of the density anisotropy parameter and the gravity

In the subAlfvénic and transAlfvénic region a smaller value of $\delta\nu^2$ reduces the gradient of the velocity (see Sect. 3.1) and the base of the wind is shifted inwards. Furthermore, the value of $(\delta\nu^2)_o$ decreases by raising λ: this trend is related to the fact that the larger is λ the more centrifugally driven is the wind, so that the thermal contribution to the acceleration ($\propto \delta\nu^2$) can be reduced. As the asymptotic Alfvén number does not depend on $\delta\nu^2$, we also expect that, by decreasing $\delta\nu^2$, the bumps have a smaller amplitude in the transition regions, with a narrower gap between the bumpy and monotonically increasing solutions.

These features appear evident in Fig. 5 where we have plotted the numerical solutions assuming $\delta\nu^2 = (\delta\nu^2)_o$ for $\lambda = 0.3$ and $\lambda = 3$. We have found $(\delta\nu^2)_o \approx 4.6$ with $R_o = 0.46$ for $\lambda = 0.3$, and $(\delta\nu^2)_o = 1.4$ with $R_o = 0.14$ for $\lambda = 3$ (in both cases $\theta_{out} \approx 73^o - 74^o$). In the former case we find $q_s = 9.3 \times 10^{-6}$ and $q' = -3.1 \times 10^{-5}$ while for $\lambda = 3$ it is $q_s = 4.2 \times 10^{-6}$ and $q' = 1.3 \times 10^{-6}$. It is interesting to note that the position where the asymptotic region begins is basically not affected by the values of $\delta\nu^2$. The almost disappearence of the bumps for fast rotation and low values of $\delta\nu^2$ is also evident, as discused in the previous paragraph.

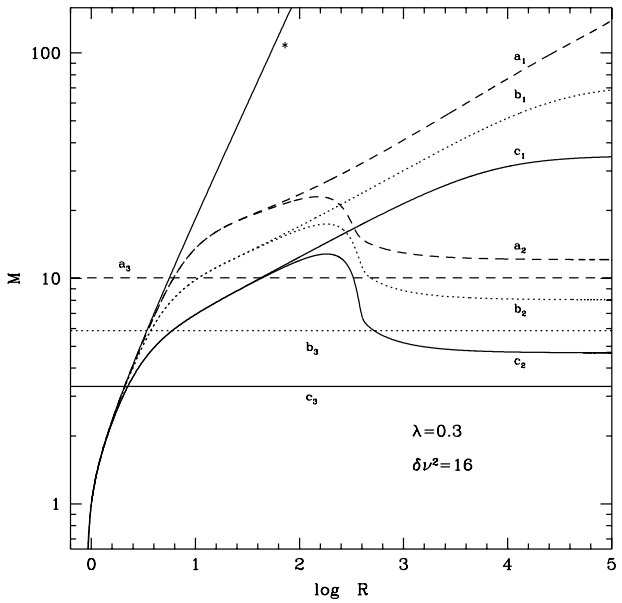

Fig. 7. Plot of M *vs* the dimensionless radial distance R along the polar axis for $\lambda = 0.3$, $\delta\nu^2 = 16$ and different values of the collimation parameter: $a = 0.1$ (solid lines), $a = 0.03$ (dotted lines), $a = 0.01$ (dashed lines), $a = 0$ (solid line, marked with a star). For each case the monotonically increasing solutions are plotted: a_1 ($q_s = 1.2 \times 10^{-9}$), b_1 ($q_s = 9.8 \times 10^{-8}$), c_1 ($q_s = 5.6 \times 10^{-6}$); one of the bumpy solutions: a_2 ($q = -9.3 \times 10^{-5}$), b_2 ($q = -4.6 \times 10^{-4}$), c_2 ($q = -3.7 \times 10^{-3}$); and $M(q = q_{min})$: a_3 ($q_{min} = -0.0165$), b_3 ($q_{min} = -1.69 \times 10^{-3}$), c_3 ($q_{min} = -1.95 \times 10^{-4}$).

Concerning the general trend with λ and $\delta\nu^2$, we have verified that a scaling of these parameters is present in the solutions. If λ is multiplied and $\delta\nu^2$ divided by the same factor (or vice versa), the asymptotic region is attained closer (or farther) to the base by almost the same factor. However the structure of the solutions (i.e. M, q' and q_s), scaled on the distance, appears almost identical. This is related to the behaviour of the solutions in the subAlfvénic and transAlfvénic regions: for smaller λ and $\delta\nu^2$ the slope of M^2 is steeper at $R \approx R_o$ and flatter at $R = 1$. This is shown in Fig. 6 by comparing the two solutions for $\lambda = 0.3$, $\delta\nu^2 = 16$ (upper panel, solution c) and $\lambda = 3$, $\delta\nu^2 = 160$ (lower panel, solution a). Consistently we find $R_o = 0.85$ in the former case and $R_o = 0.55$ in the latter case.

We remark finally that the monotonically increasing solutions have asymptotic Alfvén numbers increasing with $\delta\nu^2$, an opposite trend with respect to the value of λ. This is expected because an increase of $\delta\nu^2$ rises the thermal contribution to the acceleration. In particular, for slow rotation the asymptotic Alfvén number rapidly increases with $\delta\nu^2$ along the upper branch of Fig. 1 and q_s decreases. For fast rotating objects and $\delta\nu^2 \approx (\delta\nu^2)_o$, M_∞ is on the lower (magnetic) branch with $q_s < q_{max}$. By rising $\delta\nu^2$, M_∞ slowly increases until $q_s \to q_{max}$, then for a further increase of $\delta\nu^2$ the Alfvén number "turns around" and shifts on the upper (thermal) branch, and behaves as in the slow rotation case. This trend becomes evident in the plots of Fig. 6.

4.3. Different widths of a collimated wind

In Sect. 3 we have studied the effect of the width of the jet on the flow dynamics in the asymptotic regime. The lower is a the higher is the Alfvén number for $R \gg 1$ (Fig. 1), while in the subAlvfénic and transAlfvénic region, where the streamlines are basically radial, the solutions are almost unaffected by the value of a. By increasing the beam width indefinitely ($a \to 0$) the solutions "relax" towards the one obtained for radial flows (TT91). This trend is confirmed by the numerical results shown in Fig. 7, where we draw the monotonically increasing solution and a bumpy solution for $\lambda = 0.3$, $\delta\nu^2 = 16$, and $a = 0.1,\ 0.03,\ 0.01,\ 0$, respectively.

Concerning the monotonically increasing solution, we must remark that an increase of the outflow width means a more efficient acceleration process, thence the asymptotic region is reached farther away from the Alfvén surface. For $a = 0.01$ this occurs at distances $R > 10^5$, and for $a \to 0$ it disappears, since the flow velocity increases slowly but indefinitely (TT91). We further note that the value of q_s decreases with a, as expected from Fig. 1.

For the bumpy solutions, by decreasing a we can keep unchanged the asymptotic value of M_∞ by rising the value of $|q|$ (see Fig. 1, $q < 0$). However the increase of $|q|$ shifts upwind the position of the bump, such that the smaller is a, the closer to the Alfvén surface the asymptotic regime is reached. On the other hand the lowest allowed value of M, which is $M(q = q_{min})$, increases with the beam width. So decreasing a will raise the asymptotic Alfvén numbers that solutions can reach. As final cumulative effect of these opposite trends, the shape of solutions with M_∞ slightly above $M(q = q_{min})$ is not affected qualitatively by increasing the beam width (see Fig. 7). Furthermore, the region of the bumps is shifted slowly downstream, so that, in the limit $a \to 0$, $M(q = q_{min}) \to \infty$ and the bumpy solutions disappear.

4.4. Thermodynamics of the flow: pressure, density, temperature, heating

The pressure distribution along a streamline depends on the value of Q_o, whose value at infinity must be selected such that all along the flow the total pressure is positive. The fulfilment of this condition must take into account that: i) the contribution of the term Q_1 to the total pressure (Eq. 2.9) may be negative; ii) at the position of the bumps, the term Q_o reaches a minimum value which can become negative, as in the case of ST94 for strong oscillations. We have tested numerically the behaviour of the pressure for some representative values of the parameters. In Figs. 8 and 9 we plot the dimensionless pressure, temperature and density assuming $\lambda = 0.3$ and $\lambda = 3$ for the monotonically increasing solution and one of the bumpy solutions. We remind that Q_o, and then all the thermodynamic quantities, depend on the particular values of ν and δ. For sake of simplicity we have assumed $\delta\nu^2 \approx (\delta\nu^2)_o$ and fixed $\nu = 2$, so that we have $\delta = 1.16$ ($\lambda = 0.3$) and $\delta = 0.35$ ($\lambda = 3$).

For slow rotation, $\lambda = 0.3$, in the monotonically increasing solution the pressure is monotonically decreasing at a rate that

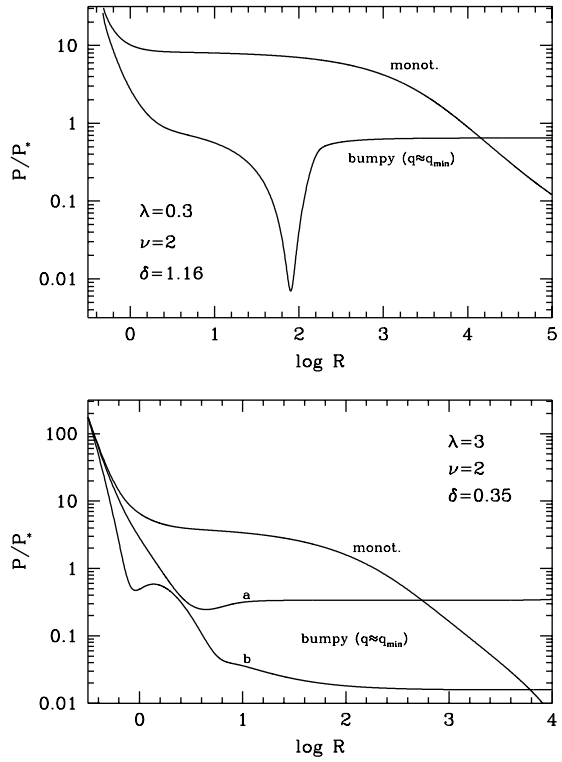

Fig. 8. Plots of the pressure P (in units of $P_* \equiv \rho_* V_*^2/2$, see Eq. 2.9) *vs.* the dimensionless radial distance R for the monotonically increasing and a bumpy solutions with $q \approx q_{min}$, $\delta\nu^2 \approx (\delta\nu^2)_o$, λ = 0.3 (upper panel) and λ = 3 (lower panel). The monotonically increasing solution is plotted along the polar axis, while the labels a and b refer to the bumpy solutions along the polar axis and on the outermost streamline, respectively.

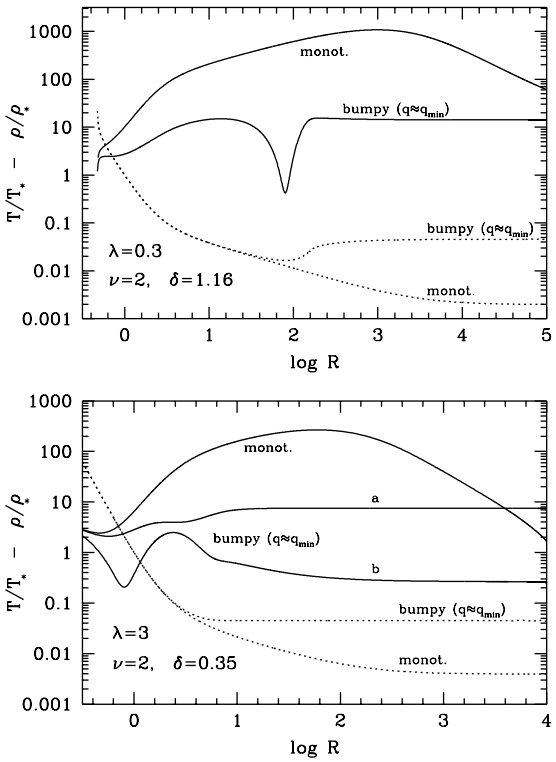

Fig. 9. Plots of the temperature T (in units of $T_* \equiv P_*/\rho_*$, solid line) and density ρ (in units of ρ_*, dotted line) *vs.* the dimensionless radial distance R, for the same solutions of Fig. 8.

depends on the value of $Q_{o,\infty}$. The value of Q_1 is positive everywhere, as expected for a low rotation velocity, therefore there is no problem in fulfiling the condition $P > 0$ everywhere along each streamline. In Fig. 8 we plot the pressure vs R assuming $Q_{o,\infty} \sim 0$. For the bumpy solutions the behaviour of P is quite different: the pressure reaches a minimum at the position of the bump, and thence rises to a constant value. To avoid negative pressure in the region of the bump, we must have $Q_{o,\infty} \geq 0.65$ for the assumed parameters, thence for this class of solutions the pressure can never vanish asymptotically, as also found in some cases of ST94.

Higher rotation velocities imply a much stronger effect of Q_1 on the total pressure, as required by the force balance across the streamlines. This is particularily important for the bumpy solutions: the value of $Q_{o,\infty}$ has a lower limit to avoid $P < 0$ not because of the depression in the bump (that now almost disappears), but because Q_1 is negative. For the assumed parameters and λ = 3 we must choose $Q_{o,\infty} \geq 0.35$. The main consequence for solutions with slow rotation is that, in the collimated region, there is a strong decrease of the pressure between the rotational axis and the outermost streamline: more than a factor 10 in our case.

The behaviour of the density vs R (Fig. 9) is easily deduced from the behaviour of the Alfvén number, if we recall that $\rho \propto 1/M^2$: it never vanishes, but attains an asymptotic value monotonically decreasing for the monotonically increasing solutions, and with a minimum for the bumpy solutions. This trend is basically unaffected by the rotational rate, apart the lack of a minimum for λ = 3. For slowly rotating flows (λ = 0.3) the temperature in the monotonically increasing solutions conversely has a maximum as it rises from the base up to the collimated region, and decreases thereafter. This means that asymptotically ($R \to \infty$) the temperature is expected to be quite low. In the bumpy solutions and for slow rotation T has a slower increase at the base and attains a constant value in the collimated region after crossing a sharp minimum in the bumpy region. For faster rotation (λ = 3) the temperature in the bumpy solutions appears quite constant all along the rotational axis, while it oscillates in the transition region ($R \gtrsim 1$) on the outermost streamline due to the effect of the term $Q_1 < 0$ on the total pressure. Note also that in the asymptotic region *the jet is hotter along the symmetry axis* than on its outer edges. This can be predicted by the pressure behaviour, taking into account that the density of the wind increases only by a factor $(1 + \delta)$ as we move away from the rotational axis.

These trends of the thermodynamical variables, which are quite general and not strongly dependent on the values of the various parameters, are consistent with the heating/losses of en-

ergy inside the plasma. The volumetric heating rate depends on the variables and their derivatives (see Eqs. 2.10), accordingly, from the asymptotic analysis of Sect. 3, we expect $\sigma \longrightarrow 0$ along all the streamlines of the wind, as M^2, Q_o and Q_1/f are constant. We have verified that in general the heating rate is monotonically decreasing from the base and vanishes in the collimated region for the monotonically increasing solutions. For the bumpy solutions σ has a negative minimum at the position of the bumps, as expected from the drop of the temperature (see also ST94).

Evidently, the behaviour of these rotating solutions is completely different with respect to that obtained for nonrotating winds analyzed in TT93. In this case of nonrotating outflows, cylindrically collimated solutions have a monotonically increasing velocity $M^2 \propto R^{1/2}$. This means that at the base of the flow Q_o should be infinite to avoid a negative pressure asymptotically, so that also the heating rate should diverge (see TT93).

5. Discussion and astrophysical applications

5.1. Summary of main results

We have performed a parametric analysis of meridionally self-similar outflows by prescribing asymptotically collimated streamlines, and assuming a nonspherically symmetric distribution for the density and gas pressure. In the region where the wind is cylindrically collimated, far from the Alfvén surface, the general physical properties of a superAlfvénic outflow are mainly ruled by the magnitude of the rotation, the gas pressure distribution and the asymptotic beam width. These properties can be summarized as follows:

I. Asymptotic confinement:
- *Overpressured jets*. They are magnetically dominated and the flow is always confined by the toroidal magnetic field, a behaviour exhibited by both, SMR and FMR. However, in slower rotators solutions also exist with larger maxima in the amplitude of the velocity and minima in the density and pressure (bumps), than those in faster rotators. These features also hold for beams with a vanishing gradient of the gas pressure across the streamlines (q = 0) where the pinching magnetic force is balanced by the centrifugal force.
- *Underpressured jets in fast magnetic rotators*. This case is similar to the previous one and the flow is always in the magnetically dominated regime, while the physical quantities have basically no intermediate bumps.
- *Underpressured jets in slow magnetic rotators*. By reducing the rotational velocity the flow enters the thermally dominated regime. The jet is confined by the gas pressure and shows a strong increase of its terminal speed.

The above results are not affected by the width of the collimated outflow. In fact, the wider is the beam the higher is its terminal speed, which increases without bound in the limit of radial streamlines.

II. Initial acceleration:
- ⋆ In the subAlfvénic and transAlfvénic zones, the acceleration is sensitive to the strength of rotation (λ) and, most crucially, on the degree of the latitudinal density anisotropy (δ), for a given central gravitating body (i.e. for a given value of ν). If the density of the gas increases as we move away from the rotational axis we may have a net acceleration, similarily to the case of nonrotating or unmagnetized winds (Tsinganos & Trussoni 1990, TT91 and TT93).
- ⋆ On the other hand, closer to the base the wind is mainly thermally driven and the gas pressure distribution between the inner and outer streamlines, Q_1, has a rather weak effect on the acceleration.

5.2. Astrophysical applications

Our main goal in this study has been the analysis of some mathematical and physical properties of meridionally self-similar collimated outflows. As we discussed in the beginning, such an analysis can be only performed under several simplifying assumptions, such as the neglect of the detailed energetics of the outflows, nonrelativistic treatment, etc. Nevertheless, we may test the astrophysical relevance of the solutions presented here by comparing them with some features of a wide class of observed astrophysical outflows. Thus, as in ST94, we confine our attention to winds observed in association with young stellar objects (YSO). These outflows have the following pertinent physical parameters, as deduced from various observations (ST94, Ray 1996),

$$m \sim 1\ M_\odot,\ r_o \sim 3\ r_\odot,\ \ \Omega \sim 7 \times 10^{-7}\ \text{rad s}^{-1},$$

$$n_\infty \sim 10^3\ \text{cm}^{-3},\ \ v_\infty \sim 400\ \text{km s}^{-1}\ .$$

The width of the collimated outflow is inferred to be of the order of the size of our planetary system, i.e., $\lesssim 10^{15}$ cm, while they appear collimated at distances $\lesssim 10^{16} - 10^{17}$ cm from the central star. Then, starting from the definitions of the non-dimensional variables and Eqs. (2.7), (2.8b) we have,

$$r_* = \frac{r_o}{R_o}\ \text{cm}\,,\ v_* \sim r_* \frac{\Omega}{\lambda}\ \text{km s}^{-1}\,,$$

$$\nu = \frac{1}{v_*}\sqrt{\frac{r_o}{r_*}}\sqrt{\frac{2\mathscr{G}m}{r_o}}\,,\ M_\infty^2 \approx \frac{1+a}{a}\,\frac{v_\infty}{v_*}\,. \tag{5.1}$$

We have seen that a transAlfvénic solution depends on a, λ, $\delta\nu^2$ and q; for assumed values of this set of parameters and a given stellar radius r_o at the base of the beam, the numerical results provide R_o, and thence r_*, v_*, ν and δ. By taking the terminal velocity of the flow v_∞ from the observations, we deduce the asymptotic Alfvén number, and from the asymptotic expression (3.5) the corresponding value of q. We can finally get the whole physical properties of the outflow at the Alfvén surface,

$$\rho_* = \rho_\infty M_\infty^2\ \text{gr cm}^{-3}\,,\ B_* = \sqrt{4\pi\rho_*}v_*\ \text{G}\,,$$

$$P_* = \frac{1}{2}\rho_* v_*^2 Q_{o,*} \text{ dyne cm}^{-2}\,,\ T_* = 6\times 10^{-9}\frac{P_*}{\rho_*}\text{ K}\,, \qquad (5.2a)$$

and in the asymptotic region,

$$B_\infty \approx \frac{a}{1+a}B_*\text{ G}\,,\ P_\infty = \frac{1}{2}\rho_* v_*^2 Q_{o,\infty}\text{ dyne cm}^{-2}\,,$$

$$T_\infty = 6\times 10^{-9}\frac{P_\infty}{\rho_\infty}\text{ K}\,, \qquad (5.2b)$$

(for the sake of simplicity we refer only to the rotational axis; it is straightforward to scale the variables on the outer streamlines). Here we will restrict our analysis to the following two typical cases:

I: $\lambda = 0.3$, $a = 0.01$, $\delta\nu^2 = 16$
II: $\lambda = 3$, $a = 0.1$, $\delta\nu^2 = 1.4$

The former case corresponds to a slow magnetic rotator with quite steep initial acceleration and large collimated width, while the second one to a narrower jet rotating faster and with a smoother acceleration rate at the base [$\delta\nu^2 \approx (\delta\nu^2)_o = 1.4$].
Case I. From the numerical solutions we obtain $R_o = 0.85$, so that from Eqs. (5.1) we have,

$$r_* = 2.5\times 10^{11}\text{ cm}\,,\ v_* = 58\text{ km s}^{-1}\,,$$

$$\nu = 5.67\,,\ \delta = 0.5\,,\ M_\infty = 26.3\,,\ q = -4\times 10^{-4}\,.$$

The width of the beam results to be $\approx 2.5\times 10^{13}$ cm, while the streamlines are collimated at a distance $r > r_*/\sqrt{a} \approx 2.5\times 10^{12}$ cm from the star. The wind speed (Fig. 10, upper panel) obtains a maximum value $\approx$ 800 km s^{-1} before reaching the asymptotic speed of $\approx$ 400 Km s^{-1} at a distance $r \approx 10^{14}$ cm; the jet is asymptotically overpressured and thence magnetically confined. For the other physical quantities we have from Eqs. (5.2),

$$\rho_* \approx 1.1\times 10^{-18}\text{ gr cm}^{-3}\,,\ B_* \approx 0.02\text{ G}\,,$$

$$P_* \approx 1.6\times 10^{-4}\text{ dyne cm}^{-2}\,,\ T_* \approx 8.4\times 10^5\text{ K}\,,$$

$$B_\infty \approx 2\times 10^{-4}\text{ G}\,,\ P_\infty \approx 2.8\times 10^{-6}\text{ dyne cm}^{-2}\,,$$

$$T_\infty \approx 1.6\times 10^7\text{ K}\,.$$

For $Q_{o,\infty}$ we have assumed the lowest allowed value to avoid negative pressures at the positions of the bump.
Case II. Now the Alfvén surface is farther from the the star with $R_o = 0.14$, while the deduced values of other parameters are,

$$r_* = 1.5\times 10^{12}\text{ cm}\,,\ v_* = 35\text{ km s}^{-1}\,,\ \nu = 1.4\,,\ \delta = 0.69\,,$$

$$M_\infty = 11.2\,,\ q = -5.1\times 10^{-5}\ .$$

The asymptotic width of the jet results to be $\approx 2.5\times 10^{13}$ cm, with streamlines collimated for $r > 4.7\times 10^{12}$ cm. In this case also the flow is overpressured and magnetically confined, but the full solution shows a negligible maximum in the intermediate region, $r \sim 2\times 10^{14}$ (see Fig. 10, lower panel). For the other quantites we find:

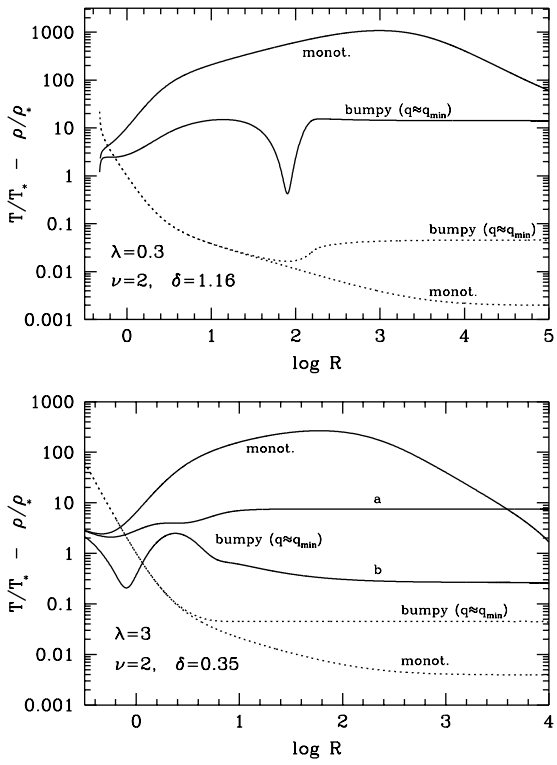

Fig. 10. Plot of the flow speed v (in km s^{-1}) *vs* the radial distance r (in cm) along the polar axis (solid line) and the outermost streamline (dashed line) for Case I ($\lambda = 0.3$, $a = 0.01$: upper panel) and Case II ($\lambda = 3$, $a = 0.1$: lower panel) of applications.

$$\rho_* \approx 1.1\times 10^{-19}\text{ gr cm}^{-3}\,,\ B_* \approx 5.4\times 10^{-3}\text{ G}\,,$$

$$P_* \approx 4.5\times 10^{-6}\text{ dyne cm}^{-2}\,,\ T_* \approx 1.4\times 10^5\text{ K}\,,$$

$$B_\infty \approx 4.9\times 10^{-4}\text{ G}\,,\ P_\infty \approx 4.8\times 10^{-8}\text{ dyne cm}^{-2}\,,$$

$$T_\infty \approx 2.4\times 10^5\text{ K}\,,$$

where we have chosen $Q_{o,\infty}$ such that the pressure is always positive on the outer streamlines ($Q_o > |Q_1|$). It must be remarked that, even though the bump in the velocity has a rather low amplitude, the corresponding jump of the thermodynamic variables is always quite large.

The values of the physical variables obtained in the two cases are roughly in agreement with the observations. It is worth to note that the magnetic field is essential for the outflow collimation. More in detail, we can say that the faster rotating solution can better describe the structure of the wind. In fact, in Case I, the velocity is quite high in the intermediate region, and the terminal temperatures large. For fast rotators the asymptotic temperature is lower, so that the required net heating of the plasma is reduced. We must also remark that the intermediate maximum in the temperature can be reduced by assuming a lower terminal speed: values of $v_\infty \approx 250 - 300$ km s^{-1} are consistent with

the observations. In such a case M_∞ is lower: $q \to q_{min}$, and the temperature is more uniform along the jet (see Fig. 9).

5.3. Conclusions

The present treatment overcomes some limitations which emerged in the studies reported in our previous articles of this series. For example, in the case of rotating flows with radial streamlines (TT91) the occurrence of negative pressures for rapidly rotating flows limited the validity of the model within a region up to a maximum colatitude. Furthermore, the terminal flow speed was unbounded. Also, for nonrotating winds full collimation cannot be attained except with an infinite input of energy in the flow (TT93). Here we have shown that both these problems do not exist if the wind is *collimated* and *rotating*.

On the other hand, some general features of the present solutions are similar to those obtained in ST94 where a spherically symmetric pressure was assumed and the pattern of the poloidal streamlines was deduced. For example, the presence of oscillations and bumps in the superAlfvénic zone is common to both cases. Also, preliminary results for solutions obtained by assuming a nonspherically symmetric gas pressure, $P_1 \propto \kappa f P_o$ with $\kappa > 0$, confirm that asymptotically the wind is collimated (Trussoni et al. 1996, Sauty et al. 1996). A detailed study of such class of solutions, and their comparison with the present results is in preparation.

Concerning the application to various astrophysical environments, we should keep in mind that our solutions are mainly valid to investigate the outflow properties along the rotational axis of the jet. Therefore the present analysis should be considered complementary to radially self-similar ones, suitable to model winds from accretion disks. The difference between these two different approaches could perhaps be reduced by assuming for the magnetic flux function $A(r,\theta)$ a more general multipole expansion in the colatitude [instead simply assuming $A(r,\theta) \propto \sin^2\theta$]. Such an approach has been already attempted for radial HD and MHD outflows (Lima & Priest 1993, Lima et al. 1996) and nonrotating MHD flows (Rotstein & Ferro Fontán 1995b). However, it is not obvious whether an extension of these studies can be performed by including rotation and collimation.

Finally, we should remark that in winds from accretion disks, the initial acceleration is mainly driven by the centrifugal force (thence the gas can be assumed 'cold'). In our case however, as we are restricted to regions close to the polar axis, the most reasonable driving mechanism cannot be other but the thermal one, so that the plasma must be 'hot' and energy addition into the flow must be present. From this point of view our scenario is rather similar to thermally driven polytropic winds, where the condition $\gamma < 5/3$ for acceleration implies heating mechanisms operating in the plasma. The nature and exact expressions for the physical processes that can heat the plasma there are an interesting and already active field of study by itself, which however lies beyond the scope of the present study.

Acknowledgements. The authors wish to thank the Foreign Offices of Greece, France and Italy for financial support. E. T. and C. S. thank the Department of Physics of the University of Crete for hospitality.

References

Appl S., Camenzind M., 1992, A&A, 256, 354
Appl S., Camenzind M., 1993, A&A, 270, 71
Baker G.L., Gollub J.P., 1990, *Chaotic Dynamics*, Cambridge University Press
Bardeen J.M., Berger B.K., 1978, ApJ, 221, 105
Biretta T., 1996, in *Solar and Astrophysical MHD Flows*, K. Tsinganos (ed.), Kluwer Academic Publishers, 357
Blandford R.D., Payne D.G., 1982, MNRAS, 199, 883
Contopoulos J., 1992, PhD thesis, Cornell University
Contopoulos J., 1994, ApJ, 432, 508
Ferreira J., 1997, A&A, in press
Hearn A.G., 1975, A&A, 40, 355
Heyvaerts J., Norman C.A., 1989, ApJ, 347, 1055
Kafatos M., 1996, in *Solar and Astrophysical MHD Flows*, K. Tsinganos (ed.), Kluwer Academic Publishers, 585
Li Z.-Y, Chiueh T., Begelman M.C., 1992, ApJ, 394, 459
Li Z.-Y, 1995, ApJ, 444, 848
Lima J.J., Priest E., 1993, A&A, 268, 641
Lima J.J., Tsinganos K., Priest E., 1996, Astrophys. Lett. & Comm., 34, 281
Lovelace R.V.E., Berk H.L., Contopoulos J., 1991, ApJ, 379, 696
Low B.C., Tsinganos K., 1986, ApJ, 302, 163
Mirabel I.F., Rodriguez L.F., 1996, in *Solar and Astrophysical MHD Flows*, K. Tsinganos (ed.), Kluwer Academic Publishers, 683
Mestel L., 1968, MNRAS, 138, 359
Nobili L., Turolla R., 1988, ApJ, 333, 248
Pelletier G., Pudritz R.E., 1991, ApJ, 394, 117
Ray T.P., 1996, in *Solar and Astrophysical MHD Flows*, K. Tsinganos (ed.), Kluwer Academic Publishers, 539
Rosso F., Pelletier G., 1994, A&A, 287, 325
Rotstein N.O., Ferro Fontán C., 1995a, ApJ, 449, 745
Rotstein N.O., Ferro Fontán C., 1995b, ApJ, 449, 764
Sakurai T., 1990, Computer Physics Reports, 12, 247
Sauty C., 1994, Ann. Phys. Fr., 19, 469
Sauty C., Tsinganos K., 1994, A&A, 287, 893 (ST94)
Sauty C., Tsinganos K., Trussoni E., 1996 in *Disks and Outflows around Young Stars*, S. Beckwith, J. Staude, A. Quetz and A. Natta (eds.), Lecture Notes in Physics, 435, 312
Trussoni E., Tsinganos K., 1993, A&A, 269, 589 (TT93)
Trussoni E., Sauty C., Tsinganos K., 1996, in *Solar and Astrophysical MHD Flows*, K. Tsinganos (ed.), Kluwer Academic Publishers, 383
Tsinganos K., 1982, ApJ, 252, 775
Tsinganos K., Low B.C., 1989, ApJ, 342, 1028
Tsinganos K., Sauty C., 1992a, A&A, 255, 405
Tsinganos K., Sauty C., 1992b, A&A, 257, 790
Tsinganos K., Sauty C., Surlantzis G., Trussoni E., Contopoulos J., 1996, in *Solar and Astrophysical MHD Flows*, K. Tsinganos (ed.), Kluwer Academic Publishers, 247
Tsinganos K., Trussoni E., 1990, A&A, 231, 270
Tsinganos K., Trussoni E., 1991, A&A, 249, 156 (TT91)
Tsinganos K., Trussoni E., Sauty C., 1992, in *The Sun: A laboratory of Astrophysics*, J. Brown and J. Schmeltz (eds.), Kluwer Academic Publishers, 379
Vardavas I.M., Hearn A.G., 1981, A&A, 98, 241
Weber E.J., Davis L.J., 1967, ApJ, 148, 217
Weber E.J., 1970, Sol. Phys., 14, 480
Żytkow A., 1972, Acta Astronomica, 22, 103

This article was processed by the author using Springer-Verlag LaTeX A&A style file *L-AA* version 3.